Lensfree super-resolution holographic microscopy using wetting films on a chip

Onur Mudanyali,[1] Waheb Bishara,[1] and Aydogan Ozcan[1,2,3,*]

[1] Electrical Engineering Department, University of California, Los Angeles, CA 90095, USA
[2] Bioengineering Department, University of California, Los Angeles, CA 90095, USA
[3] California NanoSystems Institute, University of California, Los Angeles, CA 90095, USA
*ozcan@ucla.edu
http://innovate.ee.ucla.edu

Abstract: We investigate the use of wetting films to significantly improve the imaging performance of lensfree pixel super-resolution on-chip microscopy, achieving < 1 µm spatial resolution over a large imaging area of ~24 mm^2. Formation of an ultra-thin wetting film over the specimen effectively creates a micro-lens effect over each object, which significantly improves the signal-to-noise-ratio and therefore the resolution of our lensfree images. We validate the performance of this approach through lensfree on-chip imaging of various objects having fine morphological features (with dimensions of e.g., ≤0.5 µm) such as Escherichia coli (E. coli), human sperm, Giardia lamblia trophozoites, polystyrene micro beads as well as red blood cells. These results are especially important for the development of highly sensitive field-portable microscopic analysis tools for resource limited settings.

© 2011 Optical Society of America

OCIS codes. (090.1995) Digital holography; (170.3880) Medical and biological imaging.

References and Links

1. W. R. Zipfel, R. M. Williams, and W. W. Webb, "Nonlinear magic: multiphoton microscopy in the biosciences," Nat. Biotechnol. **21**(11), 1369–1377 (2003).
2. S. W. Hell, "Toward fluorescence nanoscopy," Nat. Biotechnol. **21**(11), 1347–1355 (2003).
3. M. G. L. Gustafsson, "Nonlinear structured-illumination microscopy: wide-field fluorescence imaging with theoretically unlimited resolution," Proc. Natl. Acad. Sci. U.S.A. **102**(37), 13081–13086 (2005).
4. E. Betzig, G. H. Patterson, R. Sougrat, O. W. Lindwasser, S. Olenych, J. S. Bonifacino, M. W. Davidson, J. Lippincott-Schwartz, and H. F. Hess, "Imaging intracellular fluorescent proteins at nanometer resolution," Science **313**(5793), 1642–1645 (2006).
5. M. J. Rust, M. Bates, and X. Zhuang, "Sub-diffraction-limit imaging by stochastic optical reconstruction microscopy (STORM)," Nat. Methods **3**(10), 793–796 (2006).
6. S. T. Hess, T. P. K. Girirajan, and M. D. Mason, "Ultra-high resolution imaging by fluorescence photoactivation localization microscopy," Biophys. J. **91**(11), 4258–4272 (2006).
7. E. Chung, D. Kim, Y. Cui, Y.-H. Kim, and P. T. C. So, "Two-dimensional standing wave total internal reflection fluorescence microscopy: superresolution imaging of single molecular and biological specimens," Biophys. J. **93**(5), 1747–1757 (2007).
8. W. Choi, C. Fang-Yen, K. Badizadegan, S. Oh, N. Lue, R. R. Dasari, and M. S. Feld, "Tomographic phase microscopy," Nat. Methods **4**(9), 717–719 (2007).
9. R. P. J. Barretto, B. Messerschmidt, and M. J. Schnitzer, "In vivo fluorescence imaging with high-resolution microlenses," Nat. Methods **6**(7), 511–512 (2009).
10. K. Goda, K. K. Tsia, and B. Jalali, "Serial time-encoded amplified imaging for real-time observation of fast dynamic phenomena," Nature **458**(7242), 1145–1149 (2009).
11. W. Hübner, G. P. McNerney, P. Chen, B. M. Dale, R. E. Gordon, F. Y. S. Chuang, X.-D. Li, D. M. Asmuth, T. Huser, and B. K. Chen, "Quantitative 3D video microscopy of HIV transfer across T cell virological synapses," Science **323**(5922), 1743–1747 (2009).
12. M. Bonnet, A. Ramsay, W. Githui, L. Gagnidze, F. Varaine, and P. J. Guerin, "Bleach sedimentation: an opportunity to optimize smear microscopy for tuberculosis diagnosis in settings of high prevalence of HIV," Clin. Infect. Dis. **46**(11), 1710–1716 (2008).
13. T. Nakada, H. Matsuzawa, H. Igarashi, Y. Fujii, and I. L. Kwee, "In vivo visualization of senile-plaque-like pathology in Alzheimer's disease patients by MR microscopy on a 7T system," J. Neuroimaging **18**(2), 125–129 (2008).
14. D. V. Patel and C. N. J. McGhee, "In vivo confocal microscopy of corneal stromal nerves in patients with

peripheral neuropathy," Arch. Neurol. **66**(9), 1179–1180, author reply 1180 (2009).

15. M. Selvarajah, K. Nicholls, T. D. Hewitson, and G. J. Becker, "Targeted urine microscopy in Anderson-Fabry Disease: a cheap, sensitive and specific diagnostic technique," Nephrol. Dial. Transplant. (2011). doi:10.1093/ndt/gfr084.

16. T. Kojima, Y. Matsumoto, M. Dogru, and K. Tsubota, "The application of in vivo laser scanning confocal microscopy as a tool of conjunctival in vivo cytology in the diagnosis of dry eye ocular surface disease," Mol. Vis. **16**, 2457–2464 (2010).

17. A. Sartori, A. Mallet, E. Veiga, M. Bonazzi, S. Mostowy, L. Dortet, W. Baumeister, and P. Cossart, "Correlative Light/Electron Microscopy: a Tool for Investigating Infectious Diseases," MAM **15**(S2), 862 (2009).

18. Y. R. Shea, J. L. Davis, L. Huang, J. A. Kovacs, H. Masur, F. Mulindwa, S. Opus, Y. Chow, and P. R. Murray, "High sensitivity and specificity of acid-fast microscopy for diagnosis of pulmonary tuberculosis in an African population with a high prevalence of human immunodeficiency virus," J. Clin. Microbiol. **47**(5), 1553–1555 (2009).

19. S.-R. Wu, R. Loving, B. Lindqvist, H. Hebert, P. J. B. Koeck, M. Sjoberg, and H. Garoff, "Single-particle cryoelectron microscopy analysis reveals the HIV-1 spike as a tripod structure," Proc. Natl. Acad. Sci. U.S.A. **107**(44), 18844–18849 (2010).

20. B. J. Marais, W. Brittle, K. Painczyk, A. C. Hesseling, N. Beyers, E. Wasserman, D. van Soolingen, and R. M. Warren, "Use of light-emitting diode fluorescence microscopy to detect acid-fast bacilli in sputum," Clin. Infect. Dis. **47**(2), 203–207 (2008).

21. D. C. Essaka, J. White, P. Rathod, C. D. Whitmore, O. Hindsgaul, M. M. Palcic, and N. J. Dovichi, "Monitoring the uptake of glycosphingolipids in *Plasmodium falciparum*-infected erythrocytes using both fluorescence microscopy and capillary electrophoresis with laser-induced fluorescence detection," Anal. Chem. **82**(23), 9955–9958 (2010).

22. M. Krause, P. Rosch, B. Radt, and J. Popp, "Localizing and identifying living bacteria in an abiotic environment by a combination of Raman and fluorescence microscopy," Anal. Chem. **80**(22), 8568–8575 (2008).

23. S. E.-D. Hassan, S. I. Okoued, M. A. Mudathir, and E. M. Malik, "Testing the sensitivity and specificity of the fluorescence microscope (Cyscope) for malaria diagnosis," Malar. J. **9**(1), 88 (2010).

24. W. Bishara, U. Sikora, O. Mudanyali, T.-W. Su, O. Yaglidere, S. Luckhart, and A. Ozcan, "Holographic pixel super-resolution in portable lensless on-chip microscopy using a fiber-optic array," Lab Chip **11**(7), 1276–1279 (2011).

25. W. Bishara, T.-W. Su, A. F. Coskun, and A. Ozcan, "Lensfree on-chip microscopy over a wide field-of-view using pixel super-resolution," Opt. Express **18**(11), 11181–11191 (2010).

26. W. Bishara, H. Zhu, and A. Ozcan, "Holographic opto-fluidic microscopy," Opt. Express **18**(26), 27499–27510 (2010).

27. S. O. Isikman, W. Bishara, S. Mavandadi, F. W. Yu, S. Feng, R. Lau, and A. Ozcan, "Lens-free optical tomographic microscope with a large imaging volume on a chip," Proc. Natl. Acad. Sci. U.S.A. **108**(18), 7296–7301 (2011).

28. E. Cuche, F. Bevilacqua, and C. Depeursinge, "Digital holography for quantitative phase-contrast imaging," Opt. Lett. **24**(5), 291–293 (1999).

29. F. Dubois, L. Joannes, and J. C. Legros, "Improved three-dimensional imaging with a digital holography microscope with a source of partial spatial coherence," Appl. Opt. **38**(34), 7085–7094 (1999).

30. W. Xu, M. H. Jericho, I. A. Meinertzhagen, and H. J. Kreuzer, "Digital in-line holography for biological applications," Proc. Natl. Acad. Sci. U.S.A. **98**(20), 11301–11305 (2001).

31. G. Pedrini and H. J. Tiziani, "Short-coherence digital microscopy by use of a lensless holographic imaging system," Appl. Opt. **41**(22), 4489–4496 (2002).

32. L. Repetto, E. Piano, and C. Pontiggia, "Lensless digital holographic microscope with light-emitting diode illumination," Opt. Lett. **29**(10), 1132–1134 (2004).

33. T.-C. Poon, "Recent progress in optical scanning holography," J. Hologr. Speckle **1**(1), 6–25 (2004).

34. B. Javidi, I. Moon, S. K. Yeom, and E. Carapezza, "Three-dimensional imaging and recognition of microorganism using single-exposure on-line (SEOL) digital holography," Opt. Express **13**(12), 4492–4506 (2005).

35. C. J. Mann, L. F. Yu, C. M. Lo, and M. K. Kim, "High-resolution quantitative phase-contrast microscopy by digital holography," Opt. Express **13**(22), 8693–8698 (2005).

36. J. Rosen, G. Indebetouw, and G. Brooker, "Homodyne scanning holography," Opt. Express **14**(10), 4280–4285 (2006).

37. J. Garcia-Sucerquia, W. Xu, M. H. Jericho, and H. J. Kreuzer, "Immersion digital in-line holographic microscopy," Opt. Lett. **31**(9), 1211–1213 (2006).

38. G. Popescu, T. Ikeda, R. R. Dasari, and M. S. Feld, "Diffraction phase microscopy for quantifying cell structure and dynamics," Opt. Lett. **31**(6), 775–777 (2006).

39. F. Dubois, C. Yourassowsky, O. Monnom, J.-C. Legros, O. Debeir, P. Van Ham, R. Kiss, and C. Decaestecker, "Digital holographic microscopy for the three-dimensional dynamic analysis of in vitro cancer cell migration," J. Biomed. Opt. **11**(5), 054032 (2006).

40. A. Stern and B. Javidi, "Theoretical analysis of three-dimensional imaging and recognition of microorganisms using single-exposure on-line (SEOL) holographic microscope," J. Opt. Soc. Am. A **24**(1), 163–168 (2007).

41. S. S. Kou and C. J. R. Sheppard, "Imaging in digital holographic microscopy," Opt. Express **15**(21), 13640–13648 (2007).

42. J. Rosen and G. Brooker, "Non-scanning motionless fluorescence three-dimensional holographic microscopy," Nat. Photonics **2**(3), 190–195 (2008).

43. U. Gopinathan, G. Pedrini, and W. Osten, "Coherence effects in digital in-line holographic microscopy," J. Opt. Soc. Am. A **25**(10), 2459–2466 (2008).
44. V. Mico, Z. Zalevsky, C. Ferreira, and J. García, "Superresolution digital holographic microscopy for three-dimensional samples," Opt. Express **16**(23), 19260–19270 (2008).
45. M. Paturzo, F. Merola, S. Grilli, S. De Nicola, A. Finizio, and P. Ferraro, "Super-resolution in digital holography by a two-dimensional dynamic phase grating," Opt. Express **16**(21), 17107–17118 (2008).
46. N. T. Shaked and J. Rosen, "Multiple-viewpoint projection holograms synthesized by spatially incoherent correlation with broadband functions," J. Opt. Soc. Am. A **25**(8), 2129–2138 (2008).
47. D. J. Brady, K. Choi, D. L. Marks, R. Horisaki, and S. Lim, "Compressive holography," Opt. Express **17**(15), 13040–13049 (2009).
48. T. R. Hillman, T. Gutzler, S. A. Alexandrov, and D. D. Sampson, "High-resolution, wide-field object reconstruction with synthetic aperture Fourier holographic optical microscopy," Opt. Express **17**(10), 7873–7892 (2009).
49. L. Waller, Y. Luo, S. Y. Yang, and G. Barbastathis, "Transport of intensity phase imaging in a volume holographic microscope," Opt. Lett. **35**(17), 2961–2963 (2010).
50. N. T. Shaked, T. M. Newpher, M. D. Ehlers, and A. Wax, "Parallel on-axis holographic phase microscopy of biological cells and unicellular microorganism dynamics," Appl. Opt. **49**(15), 2872–2878 (2010).
51. D. Bonn, J. Eggers, J. Indekeu, J. Meunier, and E. Rolley, "Wetting and spreading," Rev. Mod. Phys. **81**(2), 739–805 (2009).
52. P. de Gennes, "Wetting: statics and dynamics," Rev. Mod. Phys. **57**(3), 827–863 (1985).
53. V. M. Starov, M. G. Velarde, and C. J. Radke, *Wetting and Spreading Dynamics* (CRC Press, 2007).
54. N. A. Stelmashenko, J. P. Craven, A. M. Donald, E. M. Terentjev, and B. L. Thiel, "Topographic contrast of partially wetting water droplets in environmental scanning electron microscopy," J. Microsc. **204**(2), 172–183 (2001).
55. Q. F. Wei, R. R. Mather, A. F. Fotheringham, and R. D. Yang, "Dynamic Wetting of Fibers Observed in an Environmental Scanning Electron Microscope," Text. Res. J. **73**(6), 557–561 (2003).
56. E. Bormashenko, Y. Bormashenko, T. Stein, G. Whyman, R. Pogreb, and Z. Barkay, "Environmental scanning electron microscopy study of the fine structure of the triple line and cassie-wenzel wetting transition for sessile drops deposited on rough polymer substrates," Langmuir **23**(8), 4378–4382 (2007).
57. C. P. Allier, G. Hiernard, V. Poher, and J. M. Dinten, "Bacteria detection with thin wetting film lensless imaging," Biomed. Opt. Express **1**(3), 762–770 (2010).
58. C. P. Allier, V. Poher, J. G. Coutard, G. Hiernard, and J. M. Dinten, "Thin wetting film lensless imaging," in Proceedings of the SPIE (2011), pp. 790608–790608–8.
59. O. Mudanyali, D. Tseng, C. Oh, S. O. Isikman, I. Sencan, W. Bishara, C. Oztoprak, S. Seo, B. Khademhosseini, and A. Ozcan, "Compact, light-weight and cost-effective microscope based on lensless incoherent holography for telemedicine applications," Lab Chip **10**(11), 1417–1428 (2010).
60. S. Seo, S. O. Isikman, I. Sencan, O. Mudanyali, T.-W. Su, W. Bishara, A. Erlinger, and A. Ozcan, "High-throughput lens-free blood analysis on a chip," Anal. Chem. **82**(11), 4621–4627 (2010).
61. O. Mudanyali, C. Oztoprak, D. Tseng, A. Erlinger, and A. Ozcan, "Detection of waterborne parasites using field-portable and cost-effective lensfree microscopy," Lab Chip **10**(18), 2419–2423 (2010).
62. T.-W. Su, A. Erlinger, D. Tseng, and A. Ozcan, "Compact and light-weight automated semen analysis platform using lensfree on-chip microscopy," Anal. Chem. **82**(19), 8307–8312 (2010).
63. D. Tseng, O. Mudanyali, C. Oztoprak, S. O. Isikman, I. Sencan, O. Yaglidere, and A. Ozcan, "Lensfree microscopy on a cellphone," Lab Chip **10**(14), 1787–1792 (2010).
64. G. Stybayeva, O. Mudanyali, S. Seo, J. Silangcruz, M. Macal, E. Ramanculov, S. Dandekar, A. Erlinger, A. Ozcan, and A. Revzin, "Lensfree holographic imaging of antibody microarrays for high-throughput detection of leukocyte numbers and function," Anal. Chem. **82**(9), 3736–3744 (2010).
65. R. C. Hardie, K. J. Barnard, and E. E. Armstrong, "Joint MAP registration and high-resolution image estimation using a sequence of undersampled images," IEEE Trans. Image Process. **6**(12), 1621–1633 (1997).
66. S. C. Park, M. K. Park, and M. G. Kang, "Super-resolution image reconstruction: a technical overview," IEEE Signal Process. Mag. **20**(3), 21–36 (2003).
67. N. A. Woods, N. P. Galatsanos, and A. K. Katsaggelos, "Stochastic methods for joint registration, restoration, and interpolation of multiple undersampled images," IEEE Trans. Image Process. **15**(1), 201–213 (2006).
68. R. C. Hardie, "High-resolution image reconstruction from a sequence of rotated and translated frames and its application to an infrared imaging system," Opt. Eng. **37**(1), 247 (1998).

1. Introduction

Optical microscopy has been widely used in various fields including e.g., engineering, biology, medical diagnostics and surveillance of epidemics. Over the past decade, several novel imaging architectures have been developed to improve resolution, throughput as well as signal to noise ratio (SNR) of microscopic images [1–10]. As a result of this progress, advanced microscopy techniques have been receiving considerable attention to investigate various infectious disease markers [11–23]. However, the use of such advanced microscopy modalities has been partially limited to well-established facilities due to their relatively bulky and complex architectures as well as labor-intensive operation principles. Therefore,

screening vital signs of epidemics such as disease-marker cells, parasites or other contaminants within e.g., bodily fluids and water resources is a challenging task to perform in resource-limited field settings. Toward these goals holographic imaging in general has been emerging as a valuable platform; [24–50] and along the same lines, we have recently demonstrated field-portable lensfree pixel super-resolution microscopy [24–27] as a robust and cost–effective tool that is based on the recovery of high resolution digital in-line holograms of the objects through acquisition of multiple spatially shifted lensfree frames (see e.g., Figs. 1(b-c)). This on-chip microscopy modality is based on partially coherent illumination such that the scattered optical fields from a specimen (e.g., a cell) interfere with the un-scattered background optical field creating in-line holograms of the objects located on a given opto-electronic sensor chip. This field-portable lensless microscope [24] achieves < 1 µm resolution over a large imaging area of ~24 mm^2, which is > 100 fold larger compared to e.g., a typical 40X objective-lens. Furthermore, since it does not require any bulky optical components or precise mechanical alignment, it provides a compact and cost-effective imaging tool [24] to rapidly monitor microscopic samples even in resource limited field environments.

On the other hand, the imaging performance of this lensfree pixel super-resolution microscopy tool is still limited by our detection SNR, which may pose certain limitations for imaging of e.g., weakly scattering *phase* objects that are refractive index matched to their surrounding medium such as sub-micron bacteria in drinking water. To mitigate this limitation and significantly improve our imaging SNR and contrast, in this work we demonstrate the use of ultra-thin wetting films that effectively act as micro-lenses to enhance our on-chip imaging capabilities toward reconstruction of finer morphological features of our samples having dimensions of e.g., ≤0.5 µm.
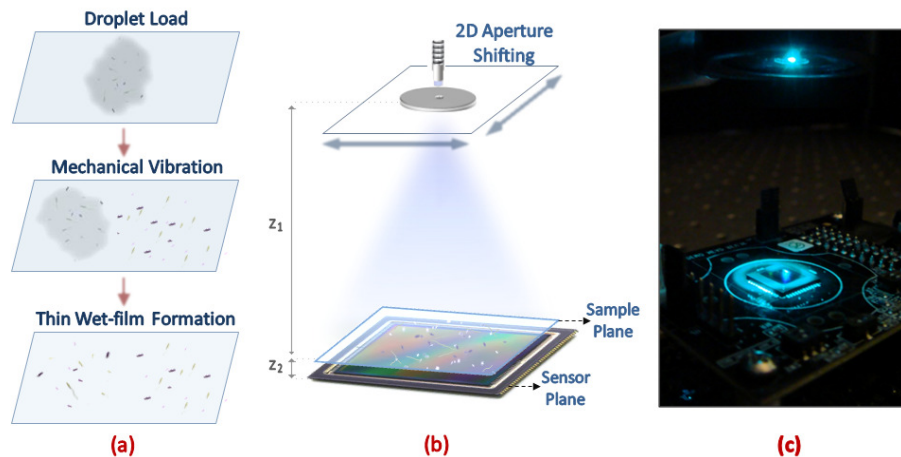

Fig. 1. (a) Schematic diagram of wetting film formation procedure (not drawn to scale). After wetting film samples were formed on plasma cleaned glass cover slips, stable micro-lens effect is verified by multiple lensfree imaging experiments spread over a day. (b) Schematic diagram of lensfree pixel super-resolution microscopy set-up (not drawn to scale). The aperture to sample plane distance (Z_1= ~10 cm) is much larger than the sample to sensor plane distance (Z_2= ~0.8-1 mm) such that discrete spatial shifts of the illumination aperture (~100 µm diameter) results in sub-pixel shifts of lensfree object holograms on the digital sensor-array. This way we can digitally reduce the effective pixel size at the sensor plane down to e.g., 0.3-0.4 µm to create higher resolution lensfree images. (c) The corresponding lensfree holographic microscopy set-up which uses a partially coherent light source that is emanating from a large aperture (D = ~100 µm). Wetting film samples were directly placed onto the CMOS sensor-chip which has an active imaging area of ~24 mm^2.

Wetting thin-film dynamics have already been widely studied in chemistry and biology [51–53] and were also utilized in imaging and sensing applications to enhance image contrast and sensitivity [54–58]. Among these prior results, a recent application of thin wetting films

towards on-chip detection of bacteria [57,58] provides a promising approach where formation of evaporation-based wetting films was used to enhance e.g., diffraction signatures of bacteria on a chip. While quite promising, this previous approach [57,58] unfortunately does not reveal microscopic images of the specimens under test since they are based on shadow imaging, and is therefore limited in scope especially for handling heterogeneous or unknown samples, where fine morphological features of the objects need to be microscopically imaged for identification and characterization purposes.

In this manuscript, we demonstrate an alternative implementation of thin wetting films on a chip that permits repeatable and reliable improvement in image quality of our field-portable lensfree super-resolution microscopes, revealing deeply sub-micron spatial features of even weakly scattering objects over a large imaging area of ~24 mm^2. We demonstrate the improved performance of our lensfree pixel super-resolution microscopy platform due to liquid-based micro-lens effect by imaging various objects on a chip such as E. coli, human sperm, Giardia lamblia trophozoites, polystyrene micro beads as well as red blood cells (RBCs). Creating a sensitive, high-resolution and wide-field micro-analysis toolset that can even work in remote or resource-poor environments, this wetting film based lensfree imaging platform could especially be important for combating global health challenges in third-world countries.

2. Overview of lensfree holographic pixel super-resolution microscopy on a chip

Imaging experiments reported in this work utilized Lensfree On-chip Pixel Super-Resolution Microscopy [24–27] that has been recently introduced by our group. This emerging lensfree on-chip imaging modality is based on partially coherent illumination (such as a simple light-emitting diode - LED) and relies on the acquisition of multiple lower resolution in-line holograms [59–64] of the objects (e.g., cells) which are spatially shifted with respect to each other by sub-pixel pitch distances (see Fig. 1). Using an iterative pixel super-resolution algorithm [24,25,65–68], these sequentially captured lensfree holograms are digitally put together, recovering a higher resolution object hologram. This super-resolved lensfree hologram is then digitally processed through a custom-developed holographic image reconstruction algorithm [24–27,59] to yield both *phase and amplitude* images of the specimens with sub-micron resolution. In this digital reconstruction process, iterative phase recovery techniques are employed such that the lost phase of the hologram at the sensor plane is recovered by propagating the optical fields back and forth between the sample and sensor planes, where at each iteration the amplitude at the sensor plane is replaced with the measured hologram amplitude whereas the phase is retained, which is gradually is refined. Once this phase recovery process converges (which typically takes ~15-20 iterations), the acquired complex wave information can be digitally back propagated to the sample plane to reveal microscopic images of the specimens with sub-micron resolution over a large field of view (FOV), e.g., 24 mm^2 [24–27,59].

Our lensfree holographic microscopy platform described above operates with unit hologram fringe magnification [24–26] to claim the entire active area of the digital sensor array as its imaging FOV. As a result of this, individual in-line holograms of the samples can be poorly sampled since each object hologram occupies a relatively small region on the sensor array. Lensfree pixel super-resolution microscopy overcomes this undersampling issue due to the limited pixel density at the sensor-array e.g., a CMOS (complementary metal-oxide-semiconductor) chip by digitally synthesizing higher resolution holograms that effectively have much smaller pixel sizes. And therefore, lensfree pixel super-resolution microscopy can achieve an effective numerical aperture (NA) of e.g., ~0.4, corresponding to sub-micron spatial resolution over an imaging area that is equivalent to the active area of the opto-electronic sensor-array (e.g., ~24 mm^2 in our case).

For our imaging experiments summarized under the Results and Discussion section, we used a quasi-monochromatic light source (500 nm center wavelength; ~5 nm bandwidth) that is emanating from a large aperture of ~100 μm diameter located at Z_1=10 cm above the digital sensor array (CMOS - Aptina MT9P031I12STM) (see Figs. 1(b-c)). The samples to be

imaged were located typically at $Z_2 < 0.8\text{-}1$ mm from the active surface of the CMOS sensor-array.

3. Sample preparation and wetting film formation

In order to mitigate SNR related limitations in partially coherent lensfree on-chip microscopy, we utilized ultra-thin wetting films which effectively act as micro-lenses over individual objects, and therefore enable significant SNR and contrast enhancement for microscopic imaging of fine spatial features of an object. Wetting film formation protocol that is described below is rather controllable and repeatable; and is therefore quite promising for practical implementations of this microscopy platform even in field settings.

Prior to preparation of wetting films, samples of interest (which were obtained from vendors or cultured in laboratory conditions) were brought to room temperature. Giardia lamblia trophozoites were fixed in 5% Formalin at pH 7.4 - 0.01% Tween 20 (Waterborne Inc., USA) and dissolved in Phosphate buffered saline (PBS). For the particular case of trophozoites, we used zinc-free pure New Methylene Blue dye (Acros Organics) that is purified with 0.45 µm pore size Syringless Filter (Whatman) for the aqueous staining of the parasites. Frozen semen samples (California Cyrobank, USA) were thawed in 37°C water bath for 10 minutes and then diluted with sperm washing medium (Irvine Scientific, USA). Whole blood samples (UCLA Blood Bank, USA) were incubated in room conditions for 30 minutes to acquire sedimented RBCs. Polystyrene beads were purchased from Thermo Scientific and E. coli specimens were cultured in UCLA Biomedical Engineering facility.

In order to form wetting films, the sample of interest is initially dissolved and agitated within 0.1 M Tris-HCl – 10% PEG 600 buffer (Sigma Aldrich) and is incubated for 30 seconds in room temperature. Using a lab pipette, a droplet of the resulting suspension (~5 µL) is placed onto a No. 1 glass cover slip (Fisher Scientific, USA) which was previously cleaned using a hand-held and field-portable plasma cleaner (Harrick Plasma). Then, the droplet is wiggled over the cover slip by gentle mechanical vibration for around 60 seconds, forming the thin wetting film over the specimen (see Fig. 1(a)). This vibration can be created simply by hand for better control of the droplet movement. It is also important to note that this procedure does not require the precise control of the droplet volume, as the wetting film spread can be easily adjusted depending on the imaging area of the CMOS sensor-array.

For comparison purposes, we also prepared traditional smear samples of E. coli and sperm (*without* the formation of thin wetting films) which we used to comparatively demonstrate the improvements of wetting films on our image quality (see e.g., Figs. 3 and 5 that will be discussed in the next section). For preparation of these conventional smears, each specimen was centrifuged for 1 minute at 3000 rpm and 2 µL of sedimented sample was dropped onto a No. 1 glass cover slip. Another cover slip was then used for smearing the droplet with an angle of ~30 degrees and air dried for ~5 minutes.

4. Experimental results and discussion

We initially demonstrated the performance of wetting films by lensless holographic imaging of Giardia lamblia trophozoites, E. coli and human RBCs (see Fig. 2). Note that some of the fine morphological features of these objects that typically have dimensions smaller than e.g., ~0.5 µm (such as the width of trophozoite flagella and the E. coli itself) generate relatively weak scattering signals and therefore their contributions to lensfree object holograms are rather limited. However, through the micro-lens effect of these wetting films, the contrast and SNR of the digital holograms of these weakly scattering features were significantly enhanced as shown in Figs. 2(a1-a6). As a result, their reconstructed lensfree microscopic images (Figs. 2(b1-b6)) successfully revealed finer features of these objects such as the flagella of Giardia lamblia trophozoites (Figs. 2(b1-b2)) as well as the unique doughnut shape of RBCs (Figs. 2(b5-b6)), providing a decent agreement to their corresponding 60X objective-lens (NA = 0.85) microscope images (Figs. 2(c1-c6)).
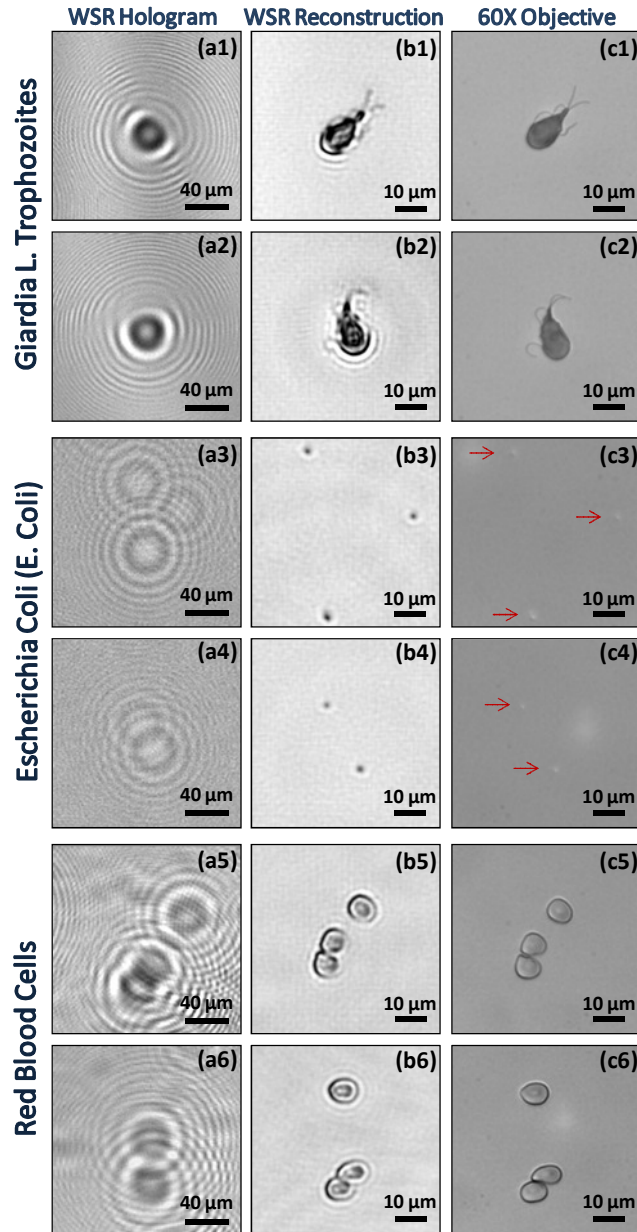
| WSR Hologram | WSR Reconstruction | 60X Objective |

Giardia L. Trophozoites

(a1) 40 µm — (b1) 10 µm — (c1) 10 µm

(a2) 40 µm — (b2) 10 µm — (c2) 10 µm

Escherichia Coli (E. Coli)

(a3) 40 µm — (b3) 10 µm — (c3) 10 µm

(a4) 40 µm — (b4) 10 µm — (c4) 10 µm

Red Blood Cells

(a5) 40 µm — (b5) 10 µm — (c5) 10 µm

(a6) 40 µm — (b6) 10 µm — (c6) 10 µm

Fig. 2. (a) Lensfree pixel super-resolution imaging results of Giardia lamblia trophozoites, E. coli and red blood cells are illustrated using thin wetting films (WSR). Digitally recovered super-resolved holograms (1st column) are reconstructed to provide their lensfree microscopic images (2nd column). 60X objective-lens (0.85 NA) bright-field microscope images of the same samples are also provided for comparison purposes (3rd column). Since E. coli samples are relatively faint in their microscope images (due to their weak scattering cross-sections), we used red arrows to point to their locations in microscope comparison images.

Note also that bright-field transmission microscope images of E. coli samples were particularly faint (even using a 0.85 NA objective-lens) due to their sub-micrometer structure; and therefore we used red arrows to point to their locations (see Figs. 2(c3-c4)). The same E. coli samples, however, were imaged with a rather strong contrast using our wetting-film based lensfree holographic microscope as illustrated in Figs. 2(b3-b4). This relative contrast

improvement compared to a regular bright-field microscope is expected since lensfree in-line holography effectively behaves like a phase contrast microscope by indirectly detecting the optical phase information of the specimens in the form of holographic intensity fringes.
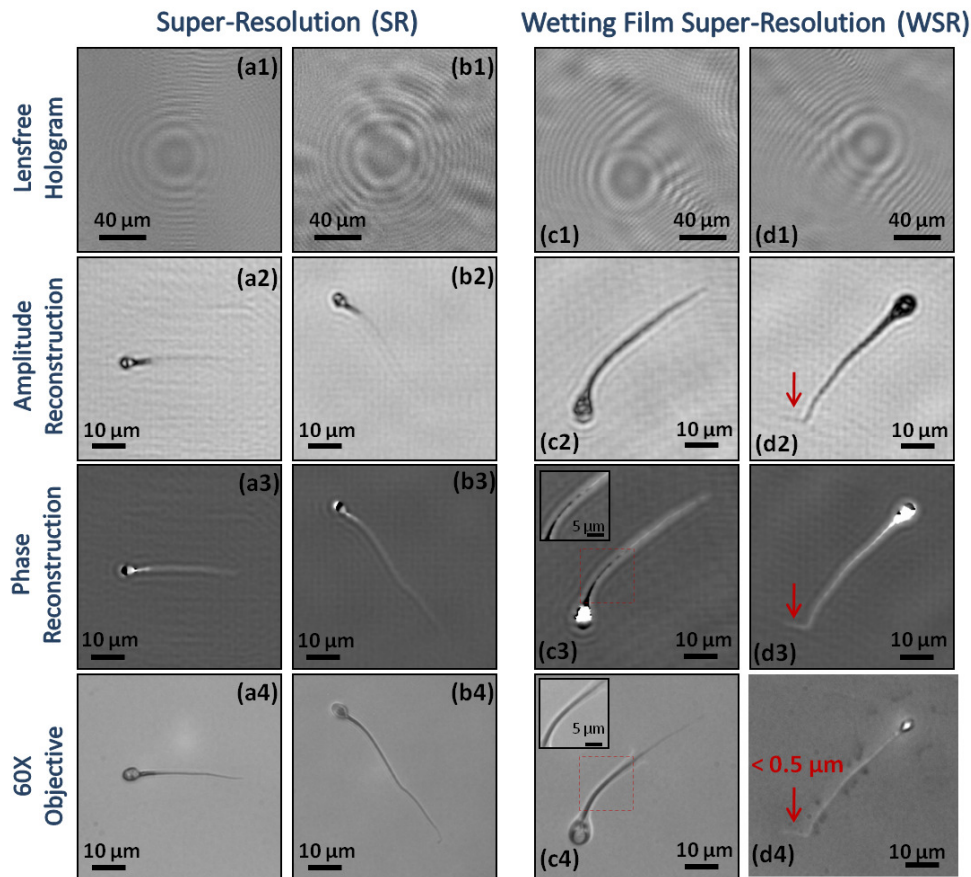

Fig. 3. Lensfree super-resolution microscopic images of sperm samples are generated using the experimental setup shown in Fig. 1(b and c). Columns (a1-a4) and (b1-b4) are obtained without the use of wetting films, while columns (c1-c4) and (d1-d4) are obtained with the thin wetting films. Significant SNR and contrast improvement in our reconstructed lensfree holographic images is observed with the thin wetting films. For example, the end of the sperm tail shown in (d4) with an arrow measures <0.5 µm in width, which was faithfully reconstructed using our wetting film based holographic microscope as illustrated in (d2) and (d3). Moreover, as shown in the digitally zoomed-in images (c3 and c4), lensfree phase recovery images revealed both the sperm tails as well as the surrounding wetting film due to the refractive index difference between two regions.

Next, to provide a better comparison of the wetting film and its effect on our imaging quality, we conducted experiments on sperm smears that were imaged using lensless pixel super-resolution microscopy *with and without* the formation of a wetting film (see Fig. 3). Without the wetting film, lensfree holograms of sperm samples did not show a major asymmetry in their fringe patterns (see Figs. 3(a1-b1)), which is due to the weaker scattering cross-sections of their tails compared to the sperm head. On the other hand, with the formation of the thin wetting film around the sperms, we observed a textural asymmetry on lensfree sperm holograms (e.g., compare Figs. 3(a1-b1) with 3(c1-d1)) which reveal the elongated holographic signatures of sperm tails due to the presence of the thin wetting film. The same conclusion was also supported in our reconstructed images (see e.g., Figs. 3(c2-d2)) such that with the wetting film the fine morphological features of the sperm tails became

much more visible compared to a regular smear without the wetting film (see Figs. 3(a2-b2)). As an example, the end of the sperm tail shown in Fig. 3(d4) with a red arrow measures <0.5 µm in width, which was faithfully imaged using our wetting film based lensless holographic microscope as illustrated in Figs. 3(d2) and 3(d3). Although the refractive index difference between the sperm tails and the surrounding medium created a sufficient contrast in our reconstructed phase images for both of the cases (i.e., with or without the use of the wetting film), phase as well as amplitude images of wetting samples were comparatively much better resolved as illustrated in Fig. 3. Notice also that the physical existence of the wetting film over the sperm samples was further validated in our phase reconstruction results, showing the tail structure recovered inside the wetting film (see e.g., the digitally zoomed region of interest in Fig. 3(c3) inset). The same behavior can be also seen in the corresponding 60X objective-lens (NA: 0.85) image as illustrated in Fig. 3(c4) and its inset.
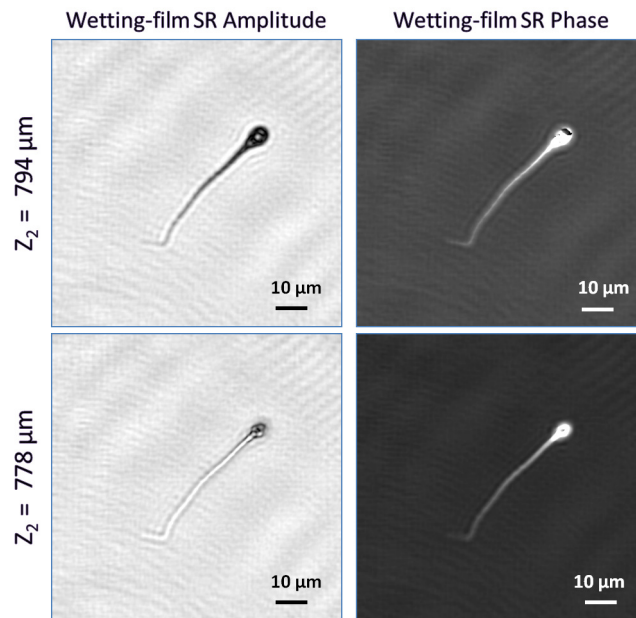

Fig. 4. By digitally changing the focusing distance (i.e., Z_2) different depths within the sample volume can be reconstructed using our lensfree super-resolution (SR) microscope. This feature is illustrated in this figure where for the same sperm sample shown in Fig. 3(d2-d3), we show two different reconstruction planes corresponding to $Z_2 = 794$ µm and 778 µm. Notice that since the wetting film induced micro-lens behaves different for the tail and the head of the sperm (due to differences in their morphology and size), we see the tail and the head get in focus at different reconstruction planes (e.g., the sperm tail is in focus at $Z_2 = 794$ µm whereas the sperm head gets in focus at $Z_2 = 778$ µm).

An important feature of lensfree holographic microscopy is that by digitally changing the focusing distance (i.e., Z_2) different depths within the sample volume can be reconstructed. This feature is illustrated in Fig. 4, where for the same sperm sample shown in Fig. 3(d2-d3), we show two different reconstruction planes corresponding to $Z_2 = 794$ µm and 778 µm. Notice that since the wetting film induced micro-lens behaves physically different for the tail and the head of the sperm (due to significant differences in their morphology and size), as expected we see the tail and the head get in focus at different reconstruction planes (e.g., the tail is in focus at $Z_2 = 794$ µm whereas the head gets in focus at $Z_2 = 778$ µm as illustrated in Fig. 4).

1 µm Bead

SNR = 17.8 dB

20 µm (a1) 5 µm (a2) 5 µm (a3) 20 µm (c1) SNR = 30.9 dB 5 µm (c2) 5 µm (c3)

E. Coli

SNR = 13.6 dB

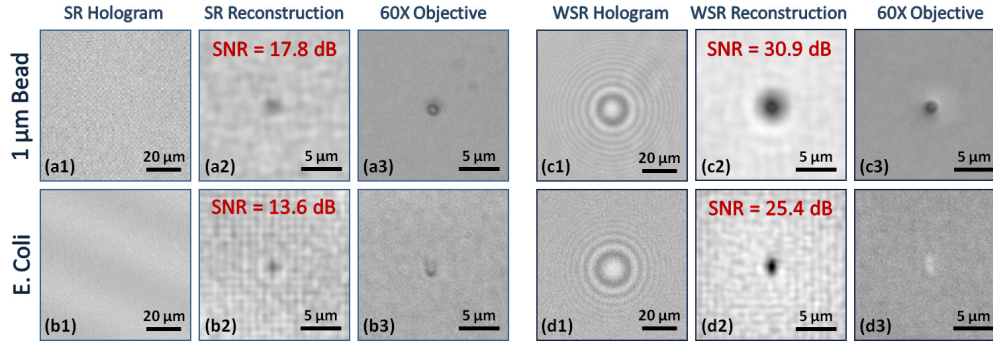20 µm (b1) 5 µm (b2) 5 µm (b3) 20 µm (d1) SNR = 25.4 dB 5 µm (d2) 5 µm (d3)

Fig. 5. 1 µm polystyrene bead and E. coli images are illustrated for both cases (Super-resolution only (SR) and Super-resolution using wetting films (WSR)) to quantify the relative SNR improvement. Using the wetting film, SNR increase of up to ~74% and ~87% in logarithmic decibel scale (corresponding to ~352% and ~289% in linear scale) is observed on lensfree amplitude reconstruction images of 1 µm bead and E. coli, respectively (see (a2) vs. (c2) and (b2) vs. (d2)). Also notice that the lensfree super-resolved holograms shown in (a1) and (b1) are not visible to bare eye since their signal intensity is quite weak without the wetting film. Despite this fact, reconstruction of these super-resolved holograms is still feasible as illustrated in (a2) and (b2), respectively.

In order to further investigate the performance improvement of our lensfree microscopy platform due to thin wetting films, we imaged a polystyrene bead of 1 µm diameter as well as an E. coli sample with and without the wetting film (see Fig. 5). First, notice that without the wetting film, the lensfree super-resolved holograms of these objects did not reveal any "visible" holographic signatures as illustrated in Figs. 5(a1-b1). Despite this fact, their reconstructed holographic images still revealed the weak signatures of these objects as illustrated in Figs. 5(a2-b2). With the use of the wetting film, however, the lensfree super resolved holograms of these particles showed a significant SNR improvement as illustrated in Figs. 5(c1-d1), where the interference fringes are rather strong and are visible to bare eye, unlike Figs. 5(a1-b1). These improved holographic signatures then translated into much better reconstructed microscopic images as shown in Figs. 5(c2-d2). These results demonstrated a significant SNR enhancement of up to ~74% and ~87% in dB (corresponding to ~352% and ~289% in linear scale) on lensfree amplitude reconstruction images of 1 µm bead and E. coli, respectively. These digital SNR values were calculated using the formula: SNR = $20\log_{10}$ |(max (I) - μ_0) / σ_0|, where I is the intensity of the reconstructed image, and μ_0 and σ_0 are the mean and the variance of the background noise region, respectively. Note also that the wetting film based lensfree reconstructed image of E. coli (Fig. 5(d2)) shows not only a higher contrast and SNR but also the elongated rod-shaped structure of the bacteria is more visible with the wetting film compared to the reconstruction results *without* the wetting film (Fig. 5(b2)).

We can qualitatively explain these observations as follows. By using a thin wetting-film, such small specimen distorts the uniform thin liquid layer that is formed on the surface such that an object dependent micro-lens structure is formed around the specimen. The main effects of this perturbed liquid layer (which occurs on and around each micro-object on the surface) are (i) to introduce a differential phase shift relative to the background light (due to thickness change in the liquid) and (ii) to cause refraction of illumination focusing some part of the light toward the specimen, which effectively increases the scattered signal strength arising from the object location. In other words, due to refraction of light rays toward the specimen, we effectively have a "condenser lens" in front of the specimen. This way the lensfree holograms of these sub-micron objects embedded within the thin wetting film will have a much better contrast and SNR. This is experimentally validated in our figures; see e.g., Fig. 5 where we compare conventional lensfree super-resolution imaging against thin wetting film performance demonstrating the significant SNR improvement due to the existence of the thin wetting film.

Finally, a full field-of-view (i.e., 24 mm^2) lensfree holographic image of a spiked wetting film sample that is composed of Giardia lamblia trophozoites, E. coli and sperm samples is illustrated in Fig. 6 in order to demonstrate the wide imaging area of this on-chip microscopy platform. Considering the additional contrast and SNR improvements due to the micro lens effect of these wetting films, such a high-throughput and high-resolution microscopy platform can be very useful to rapidly evaluate e.g., bodily fluids or water samples even in remote locations or field settings. Moreover, the wetting film formation procedure described here is rather repeatable which makes it applicable even in resource limited environments with relatively low level of training.
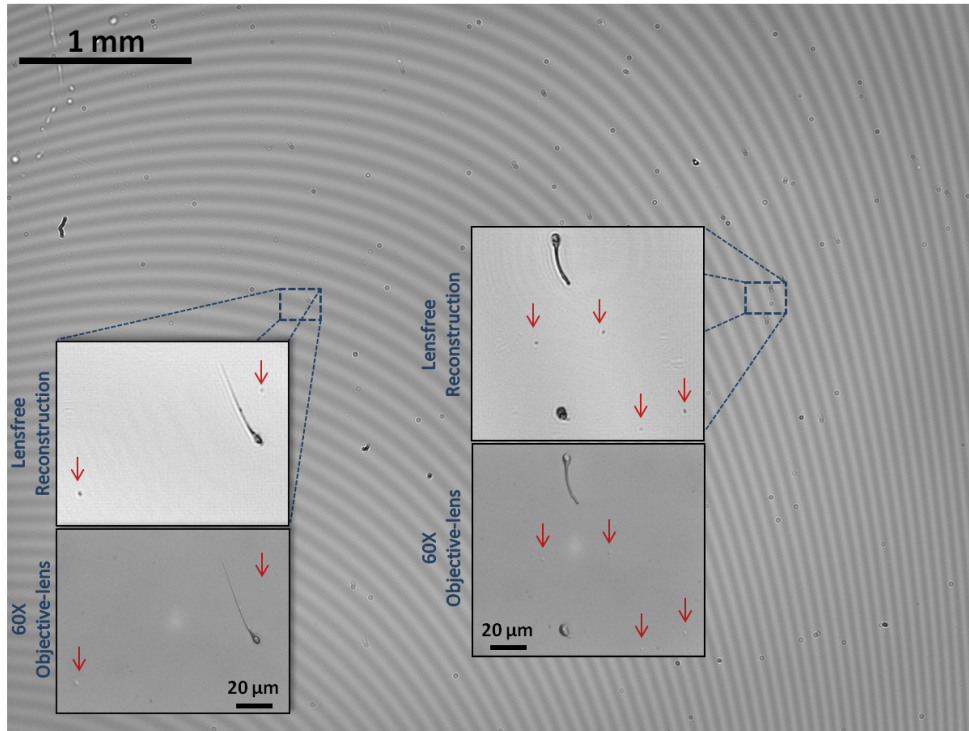

Fig. 6. Wide-field (FOV ~24 mm^2) high-resolution imaging of a heterogeneous wetting film sample that is composed of Giardia lamblia trophozoites, E. coli and sperm is demonstrated. This constitutes >100 fold larger FOV, when compared to a bright-field optical microscope using e.g., a 40X objective-lens. For comparison purposes, conventional bright-field microscope images of zoomed-regions of interest are also provided (60X objective-lens; 0.85 NA), where E. coli samples were marked with red arrows due to their faint contrast.

5. Conclusions

We demonstrated the performance improvement of lensfree on-chip super-resolution microscopy due to wetting film induced micro-lens effect by imaging various micro-objects such as Giardia lamblia trophozoites, human sperm, polystyrene beads, E. coli as well as RBCs. Experimental results yielded up to 4 fold SNR improvement, showing better recovery of sub-micron features of specimens such as sperm tails and flagella of Giardia lamblia parasites. This wetting film approach allows a stable and repeatable micro-lens effect on individual objects to enhance the capabilities of our field-portable lensfree holographic microscopes. Therefore, it may provide a quantitative toolset to carry out highly-sensitive measurements even in resource-limited environments without the need for advanced sample preparation procedures.

Acknowledgments